Inorg. Chem. **2006**, *45*, 1173–1183

Energy Transfer in Hybrids Based on a Thiophene-Substituted Ethynylbipyridine Dimer Decorated with Re(I), Ru(II), and Os(II) Units

Sébastien Goeb,[†] Antoinette De Nicola,[†] Raymond Ziessel,*[,†] Cristiana Sabatini,[‡] Andrea Barbieri,[‡] and Francesco Barigelletti*[,‡]

Istituto per la Sintesi Organica e la Fotoreattività, Consiglio Nazionale delle Ricerche (ISOF-CNR), Via P. Gobetti 101, 40129 Bologna, Italy, and Laboratoire de Chimie Moléculaire, école de Chimie, Polymères, Matériaux (ECPM), Université Louis Pasteur (ULP), 25 rue Becquerel, 67087 Strasbourg Cedex 02, France

Received October 5, 2005

The preparation, structural features, electrochemical behavior, and optical properties (at room temperature and at 77 K) are reported for a series of thiophene-containing hybrids based on the bent conjugated backbone of a rigid ditopic ligand, the dimeric moiety 3,4-dibutyl-2,5-bis{5′-[(3,4-dibutylthien-2-ylethynyl)-2,2′-bipyridin-5-yl]ethynyl}-thiophene (**TBTBT**). Within the dimer, the diethynyl-2,2′-bipyridine units (bpy, the coordination sites) alternate with three 3,4-dibuthylthiophene units and coordination of the $[Re(CO)_3Cl]$, $[Ru(bpy)_2]^{2+}$, and $[Os(bpy)_2]^{2+}$ centers results in the mononuclear species Ru**TBTBT** and Os**TBTBT** and the binuclear species Ru**TBTBT**Ru, Os**TBTBT**Os, Ru**TBTBT**Os, and Re**TBTBT**Os. At room temperature, the emitting states obtained by photoexcitation are of ^{3}MLCT nature, and vibronic analysis of the emission spectra indicates that they are largely delocalized over the **TBTBT** ligand. In the binuclear species, the intermetal separation is ca. 17 Å, and for Ru**TBTBT**Os, an efficient Ru → Os excitation transfer takes place, resulting solely in an Os-based emission. The process is ascribed to double-electron transfer (Dexter), as mediated by the **TBTBT** ligand; a similar conclusion holds for the case of Re**TBTBT**Os. For Ru**TBTBT**Os, the process is discussed in some detail also with regard to the possibility of disentangling the constituent hole and electron-transfer events.

Introduction

Thiophene-containing metallo-supramolecular oligomers and polymers incorporating photoactive and electroactive Ru(II) and Os(II) centers are an attractive class of hybrid materials that show interesting electrooptical properties.[1−10] Perspectives for the use of such materials have to do with the development of electroluminescent devices[11−14] and of devices based on elaborate sensory signal amplification[15,16] and, on general grounds, with the exploitation of their conductive properties for molecular electronics.[17−20] It is of relevance that the study of such hybrids can take advantage of the results from investigations both of Ru(II)- and Os-

* To whom correspondence should be addressed. E-mail: ziessel@chimie.u-strasbg.fr (R.Z.), franz@isof.cnr.it (F.B.).
[†] Istituto ISOF-CNR.
[‡] Université Louis Pasteur.

(1) Trouillet, L.; De Nicola, A.; Guillerez, S. *Chem. Mater.* **2000**, *12*, 1611.
(2) Wolf, M. O. *Adv. Mater.* **2001**, *13*, 545.
(3) Liu, Y.; Li, Y.; Schanze, K. S. *J. Photochem. Photobiol. C* **2002**, 1.
(4) Hjelm, J.; Handel, R. W.; Hagfeldt, A.; Constable, E. C.; Housecroft, C. E.; Forster, R. J. *J. Phys. Chem. B* **2003**, *107*, 10431.
(5) Figgemeier, E.; Merz, L.; Hermann, B. A.; Zimmermann, Y. C.; Housecroft, C. E.; Guntherodt, H. J.; Constable, E. C. *J. Phys. Chem. B* **2003**, *107*, 1157.
(6) Stott, T. L.; Wolf, M. O. *Coord. Chem. Rev.* **2003**, *246*, 89.
(7) Tor, Y. *C. R. Chim.* **2003**, *6*, 755.
(8) Coe, B. J.; Curati, N. R. M. *Comments Inorg. Chem.* **2004**, *25*, 147.
(9) Moorlag, C.; Wolf, M. O.; Bohne, C.; Patrick, B. O. *J. Am. Chem. Soc.* **2005**, *127*, 6382.
(10) Hjelm, J.; Handel, R. W.; Hagfeldt, A.; Constable, E. C.; Housecroft, C. E.; Forster, R. J. *Inorg. Chem.* **2005**, *44*, 1073.
(11) Mitschke, U.; Bäuerle, P. *J. Mater. Chem.* **2000**, *10*, 1471.
(12) Rudmann, H.; Shimada, S.; Rubner, M. F. *J. Am. Chem. Soc.* **2002**, *124*, 4918.
(13) Slinker, J.; Bernards, D.; Houston, P. L.; Abruna, H. D.; Bernhard, S.; Malliaras, G. G. *Chem. Commun.* **2003**, 2392.
(14) Holder, E.; Langeveld, B. M. W.; Schubert, U. S. *Adv. Mater.* **2005**, *17*, 1109.
(15) Swager, T. M. *Acc. Chem. Res.* **1998**, *31*, 201.
(16) Holliday, B. J.; Swager, T. M. *Chem. Commun.* **2005**, 23.
(17) Tour, J. M. *Acc. Chem. Res.* **2000**, *33*, 791.
(18) Ong, B. S.; Wu, Y. L.; Liu, P.; Gardner, S. *J. Am. Chem. Soc.* **2004**, *126*, 3378.
(19) Figgemeier, E.; Aranyos, V.; Constable, E. C.; Handel, R. W.; Housecroft, C. E.; Risinger, C.; Hagfeldt, A.; Mukhtar, E. *Inorg. Chem. Commun.* **2004**, *7*, 117.
(20) Facchetti, A.; Deng, Y.; Wang, A. C.; Koide, Y.; Sirringhaus, H.; Marks, T. J.; Friend, R. H. *Angew. Chem., Int. Ed.* **2000**, *39*, 4547.

10.1021/ic051717w CCC: $33.50
Published on Web 01/10/2006

(II)-containing multimetallic species[21−31] and of thiophene-based oligomers,[32−37] which lay relevant premises for developing approaches for their integration. Along these lines, the use of neutral Re(I) chromophores as energy donors has been somewhat neglected.

Several bi- and polymetallic species have been studied in which the metal-based units appear as terminals of an oligothiophene connecting unit.[10,38−48] In these hybrid wires, when in the presence of heterometallic species, i.e, of both Ru(II)- [or Re(I)-] and Os(II)-based centers, it is possible to study the photoinduced end-to-end excitation transfer (here represented as Ru → Os). This approach affords one way for monitoring the conductive properties of the intervening oligothiophene fragment. This is particularly useful when a series of compounds incorporating oligomers with variable length are available.[49−53]

Chart 1. Ligand and Complexes[a]

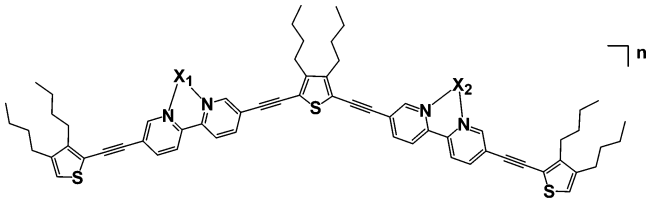

	X_1	X_2	n
TBTBT	-	-	0
Ru	$Ru(bpy)_2$		2+
RuRu	$Ru(bpy)_2$	$Ru(bpy)_2$	4+
Os	$Os(bpy)_2$		2+
OsOs	$Os(bpy)_2$	$Os(bpy)_2$	4+
RuOs	$Ru(bpy)_2$	$Os(bpy)_2$	4+
ReOs	$Re(CO)_3Cl$	$Os(bpy)_2$	2+

[a] Because of possible rotations around the various single bonds at the **TBTBT** ligand, a distribution of geometries is expected.

In this work, we assess the electrooptical properties of the series of transition-metal thiophene-containing hybrids schematically illustrated in Chart 1.[54] In this series, the electroactive and photoactive metal-based units are coupled to the bent conjugated backbone of a ditopic ligand, 3,4-dibutyl-2,5-bis{5′-[(3,4-dibutylthien-2-ylethynyl)-2,2′-bipyridin-5-yl]-ethynyl}thiophene (labeled **TBTBT**), where two 5,5′-diethynyl-2,2′-bipyridine moieties (the coordination sites) alternate with three 3,4-dibuthylthiophene units; bpy is 2,2′-bipyridine. The synthetic strategy has been devised in such a way that the end-capping of the chelating centers by a 3,4-dibutyl-2-ethynylthiophene stopper ensures the absence of dissymmetry in the bridging subunit. The dibutylalkyl chains provide a good solubility of the ligand during the complexation procedure with the metal precursors. The rigidity of the ligand is due to incorporation of ethynyl units. According to a proposed classification,[2] this relatively uncommon geometry for the resulting hybrids could be termed of type II (metal centers coupled to the oligomeric backbone), with cases where the metal groups are tethered (uncoupled) at the oligomeric backbone being of type I and those where the metal centers are included within the backbone being of type III. We describe the syntheses, structural features, electrochemical behavior, and optical properties of a series of hybrids including (i) the mononuclear complexes, Ru**TBTBT** (**Ru)** and Os**TBTBT** (**Os**), (ii) the binuclear homometallic complexes, Ru**TBTBT**Ru (**RuRu**) and Os**TBTBT**Os (**OsOs**), and (iii) the binuclear heterometallic complexes, Ru**TBTBT**Os (**RuOs**) and Re**TBTBT**Os (**ReOs**) (Chart 1). Finally we discuss in some detail the excitation transfer event

(21) Sauvage, J. P.; Collin, J. P.; Chambron, J. C.; Guillerez, S.; Coudret, C.; Balzani, V.; Barigelletti, F.; Decola, L.; Flamigni, L. *Chem. Rev.* **1994**, *94*, 993.
(22) Balzani, V.; Juris, A.; Venturi, M.; Campagna, S.; Serroni, S. *Chem. Rev.* **1996**, *96*, 759.
(23) Balzani, V.; Campagna, S.; Denti, G.; Juris, A.; Serroni, S.; Venturi, M. *Acc. Chem. Res.* **1998**, *31*, 26.
(24) Anderson, P. A.; Keene, F. R.; Meyer, T. J.; Moss, J. A.; Strouse, G. F.; Treadway, J. A. *J. Chem. Soc., Dalton Trans.* **2002**, 3820.
(25) Laine, P.; Bedioui, F.; Ochsenbein, P.; Marvaud, V.; Bonin, M.; Amouyal, E. *J. Am. Chem. Soc.* **2002**, *124*, 1364.
(26) Adams, D. M.; Brus, L.; Chidsey, C. E. D.; Creager, S.; Creutz, C.; Kagan, C. R.; Kamat, P. V.; Lieberman, M.; Lindsay, S.; Marcus, R. A.; Metzger, R. M.; Michel-Beyerle, M. E.; Miller, J. R.; Newton, M. D.; Rolison, D. R.; Sankey, O.; Schanze, K. S.; Yardley, J.; Zhu, X. Y. *J. Phys. Chem. B* **2003**, *107*, 6668.
(27) Wang, X. Y.; Del Guerzo, A.; Schmehl, R. H. *J. Photochem. Photobiol. C* **2004**, *5*, 55.
(28) Vaduvescu, S.; Potvin, P. G. *Eur. J. Inorg. Chem.* **2004**, 1763.
(29) Huynh, M. H. V.; Dattelbaum, D. M.; Meyer, T. J. *Coord. Chem. Rev.* **2005**, *249*, 457.
(30) Puntoriero, F.; Serroni, S.; Galletta, M.; Juris, A.; Licciardello, A.; Chiorboli, C.; Campagna, S.; Scandola, F. *ChemPhysChem* **2005**, *6*, 129.
(31) Low, P. J. *Dalton Trans.* **2005**, 2821.
(32) Bäuerle, P. In *Electronic Materials: The Oligomeric Approach*; Müllen, K., Wegner, G., Eds.; Wiley-VCH: Weinheim, Germany, 1998; Chapter 2.
(33) Chan, H. S. O.; Ng, S. C. *Prog. Polym. Sci.* **1998**, *23*, 1167.
(34) Roncali, J. *Acc. Chem. Res.* **2000**, *33*, 147.
(35) Otsubo, T.; Aso, Y.; Takimiya, K. *J. Mater. Chem.* **2002**, *12*, 2565.
(36) Melucci, M.; Gazzano, M.; Barbarella, G.; Cavallini, M.; Biscarini, F.; Maccagnani, P.; Ostoja, P. *J. Am. Chem. Soc.* **2003**, *125*, 10266.
(37) Barbarella, G.; Melucci, M.; Sotgiu, G. *Adv. Mater.* **2005**, *17*, 1581.
(38) Zhu, S. S.; Kingsborough, R. P.; Swager, T. M. *J. Mater. Chem.* **1999**, *9*, 2123.
(39) Constable, E. C.; Housecroft, C. E.; Schofield, E. R.; Encinas, S.; Armaroli, N.; Barigelletti, F.; Flamigni, L.; Figgemeier, E.; Vos, J. G. *Chem. Commun.* **1999**, 869.
(40) Walters, K. A.; Trouillet, L.; Guillerez, S.; Schanze, K. S. *Inorg. Chem.* **2000**, *39*, 5496.
(41) Pappenfus, T. M.; Mann, K. R. *Inorg. Chem.* **2001**, *40*, 6301.
(42) Encinas, S.; Flamigni, L.; Barigelletti, F.; Constable, E. C.; Housecroft, C. E.; Schofield, E. R.; Figgemeier, E.; Fenske, D.; Neuburger, M.; Vos, J. G.; Zehnder, M. *Chem.—Eur. J.* **2002**, *8*, 137.
(43) Liu, Y.; De Nicola, A.; Reiff, O.; Ziessel, R.; Schanze, F. S. *J. Phys. Chem. A* **2003**, *107*, 3476.
(44) Cunningham, G. B.; Li, Y. T.; Liu, S. X.; Schanze, K. S. *J. Phys. Chem. B* **2003**, *107*, 12569.
(45) Barbieri, A.; Ventura, B.; Barigelletti, F.; De Nicola, A.; Quesada, M.; Ziessel, R. *Inorg. Chem.* **2004**, *43*, 7359.
(46) Benniston, A. C.; Harriman, A.; Lawrie, D. J.; Mayeux, A. *Phys. Chem. Chem. Phys.* **2004**, *6*, 51.
(47) Lopez, R.; Villagra, D.; Ferraudi, G.; Moya, S. A.; Guerrero, J. *Inorg. Chim. Acta* **2004**, *357*, 3525.
(48) Houarner, C.; Blart, E.; Buvat, P.; Odobel, F. *Photochem. Photobiol. Sci.* **2005**, *4*, 200.
(49) Davis, W. B.; Svec, W. A.; Ratner, M. A.; Wasielewski, M. R. *Nature* **1998**, *396*, 60.
(50) Rothe, C.; Hintschich, S.; Monkman, A. P.; Svensson, M.; Anderson, M. R. *J. Chem. Phys.* **2002**, *116*, 10503.
(51) Ringenbach, C.; De Nicola, A.; Ziessel, R. *J. Org. Chem.* **2003**, *68*, 4708.
(52) Leroy-Lhez, S.; Fages, F. *C. R. Chim.* **2005**, *8*, 1204.
(53) Ziessel, R.; Bäuerle, P.; Ammann, M.; Barbieri, A.; Barigelletti, F. *Chem. Commun.* **2005**, 802.
(54) Goeb, S.; De Nicola, A.; Ziessel, R. *J. Org. Chem.* **2005**, *70*, 1518.

Chart 2. Schematic Picture of the Energy-Minimized Ground-State Structure for **RuOs** for Which the Two Metal Centers Are Arranged According to a Transoid Geometry, with an Intermetal Distance $d \sim 17$ Å (from Standard Molecular Mechanics According to Hyperchem 7.5)

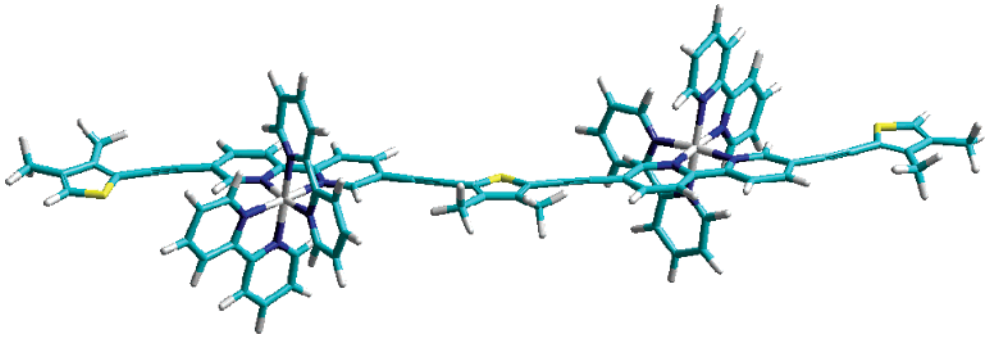

for the heterometallic species **RuOs**, for which we find a through-bridge Ru → Os excitation transmission. Chart 2 provides a schematic structure of **RuOs**, with the $[Ru(bpy)_2]^{2+}$ and $[Os(bpy)_2]^{2+}$ centers arranged in a transoid geometry with respect to the oligomeric ligand, as suggested by the results of molecular mechanics calculations.

Experimental Section

General Methods. The 200.1 (^{1}H) NMR (Bruker AC 200) spectra were recorded at room temperature using a perdeuterated solvent as the internal standard: δ (H) in ppm relative to residual protiated solvent in acetone-d_6 (2.05). Fast atom bombardment (FAB, in a positive mode) analyses were performed using a ZAB-HF-VB analytical apparatus and *m*-nitrobenzyl alcohol as the matrix. Fourier transform infrared (FT-IR) spectra were recorded on the neat liquids or as thin films, prepared with a drop of dichloromethane, and evaporated to dryness on KBr pellets. Chromatographic purification was conducted using aluminum oxide 90 standardized. Thin-layer chromatography (TLC) was performed on aluminum oxide plates coated with a fluorescent indicator. All mixtures of solvents are given in a volume-to-volume ratio. The experimental procedures for each reaction were tested several times to optimally find the best conditions. Elemental analyses (C, H, and N) were performed using an elemental analyzer (Thermo Electron Flash EA 1112, accuracy better than 0.3%).

Materials. The **TBTBT** ligand,[54] *cis*-$Cl[Ru(bipy)_2Cl_2]\cdot 2H_2O$,[55] *cis*-$Cl[Os(bipy)_2Cl_2]$,[56] and the $[Re(CO)_5Cl]$[57] metal precursors were prepared according to literature procedures.

Synthesis. Ru and RuRu Complexes. A Schlenk flask was charged with the ligand **TBTBT** (90 mg, 0.09 mmol), $[Ru(bpy)_2Cl_2]\cdot 2H_2O$ (71 mg, 0.14 mmol), and finally ethyl alcohol (30 mL). The solution was heated at 90 °C until complete consumption of the starting material (determined by TLC), and then the solvent was evaporated under vacuum. The residue was treated with a saturated aqueous solution of KPF_6 (10 mL) and extracted with dichloromethane. The organic extracts were washed with water and dried over absorbent cotton. The solvent was removed by rotary evaporation. The residue was purified by chromatography on alumina eluting with dichloromethane to dichloromethane−methyl alcohol (98.5/1.5, v/v) to give 31 mg (20%) of **Ru** as a dark-orange solid and dichloromethane−methyl alcohol (95.0/5.0, v/v) to give 109 mg (50%) of **RuRu** as a red solid.

For **Ru**: ^{1}H NMR (200 MHz, $(CD_3)_2CO$) δ 8.87−8.81 (m, 8H), 8.53 (d, 1H, ^3J = 8.3 Hz), 8.52 (d, 1H, ^3J = 8.3 Hz), 8.33−8.22 (m, 8H), 8.14 (d, 1H, ^4J = 2.1 Hz), 8.11−8.04 (m, 5H), 7.68−7.59 (m, 4H), 7.27 (s, 1H), 7.21 (s, 1H), 2.89−2.77 (m, overlapping with residual water), 2.67−2.51 (m, 8H), 1.68−1.30 (m, 24H), 1.00−0.85 (m, 18H); IR (KBr, cm^{-1}) 3125, 3086, 2956, 2931, 2870, 2196, 1595, 1466, 1447, 1373, 1243, 841; UV−vis (CH_3CN) λ nm (ϵ, M^{-1} cm^{-1}) 287 (92 000), 434 (83 500); FAB$^+$ *m*/*z* (nature of the peak, relative intensity) 1547.3 ($[M - PF_6]^+$, 100), 701.2 ($[M - 2PF_6]^{2+}$, 5). Anal. Calcd for $C_{84}H_{84}F_{12}N_8P_2RuS_3$: C, 59.60; H, 5.00; N, 6.62. Found: C, 59.40; H, 4.75; N, 6.41.

For **RuRu**: ^{1}H NMR (200 MHz, $(CD_3)_2CO$) δ 8.86−8.81 (m, 12H), 8.32−8.20 (m, 16H), 8.13−8.05 (m, 8H), 7.65−7.58 (m, 8H), 7.27 (s, 2H), 2.67−2.51 (m, 12H), 1.67−1.23 (m, 24H), 0.96−0.84 (m, 18H); IR (KBr, cm^{-1}) 3118, 3081, 2955, 2930, 2870, 2198, 1596, 1466, 1447, 1376, 1243, 841; UV−vis (CH_3CN) λ nm (ϵ, M^{-1} cm^{-1}) 288 (155 000), 444 (123 000); FAB$^+$ *m*/*z* (nature of the peak, relative intensity) 2251.2 ($[M - PF_6]^+$, 100), 1053.3 ($[M - 2PF_6]^{2+}$). Anal. Calcd for $C_{104}H_{100}F_{24}N_{12}P_4Ru_2S_3$: C, 52.13; H, 4.21; N, 7.01. Found: C, 52.06; H, 3.98; N, 7.23.

Os and OsOs Complexes. A Schlenk flask was charged with the ligand **TBTBT** (70 mg, 0.07 mmol), $[Os(bpy)_2Cl_2]$ (91 mg, 0.11 mmol), and finally ethyl alcohol (30 mL). The solution was heated at 110 °C for 4 days, and then the solvent was evaporated under vacuum. The residue was treated with a saturated aqueous solution of KPF_6 (10 mL) and extracted with dichloromethane. The organic extracts were washed with water and dried over absorbent cotton. The solvent was removed by rotary evaporation. The residue was purified by chromatography on alumina, eluting with dichloromethane to dichloromethane−methyl alcohol (97.0/3.0, v/v) to give 63 mg (50%) of **Os** as a brown solid and dichloromethane−methyl alcohol (93.0/7.0, v/v) to give 27 mg (15%) of **OsOs** as a dark-brown solid.

For **Os**: ^{1}H NMR (200 MHz, $(CD_3)_2CO$) δ 8.87−8.80 (m, 8H), 8.52 (d, 1H, ^3J = 8.2 Hz), 8.51 (d, 1H, ^3J = 8.2 Hz), 8.14−7.97 (m, 14H), 7.59−7.50 (m, 4H), 7.25 (s, 1H), 7.20 (s, 1H), 2.80 (t, 4H, ^3J = 7.5 Hz), 2.68−2.51 (m, 8H), 1.71−1.24 (m, 24H), 1.01−0.85 (m, 18H); IR (KBr, cm^{-1}) 3114, 3078, 2952, 2930, 2861, 1590, 1464, 1445, 1270, 840; UV−vis (CH_3CN) λ nm (ϵ, M^{-1} cm^{-1}) 291 (88 400), 435 (75 200), 530 (8000); FAB$^+$ *m*/*z* (nature of the peak, relative intensity) 1638.2 ($[M - PF_6]^+$), 100), 746.2 ($[M - 2PF_6]^{2+}$, 20). Anal. Calcd for $C_{84}H_{84}F_{12}N_8OsP_2S_3$: C, 56.62; H, 4.75; N, 6.29. Found: C, 56.41; H, 4.43; N, 6.02.

For **OsOs**: ^{1}H NMR (200 MHz, $(CD_3)_2CO$) δ 8.82−8.78 (m, 12H), 8.12−7.95 (m, 24H), 7.57−7.48 (m, 8H), 7.25 (s, 2H), 2.68−2.51 (m, 12H), 1.67−1.19 (m, 24H), 0.96−0.84 (m, 18H); IR (KBr, cm^{-1}) 3114, 3078, 2955, 2927, 2870, 2197, 1594, 1464, 1447, 1373, 1268, 1242, 840; UV−vis (CH_3CN) λ nm (ϵ, M^{-1} cm^{-1}) 290

(55) Sullivan, B. P.; Salmon, D. J.; Meyer, T. J. *Inorg. Chem.* **1978**, *17*, 3334.
(56) Kober, E. M.; Caspar, J. V.; Sullivan, B. P.; Meyer, T. J. *Inorg. Chem.* **1988**, *27*, 4587.
(57) Zingales, F.; Graziani, M.; Calderazzo, F. *Gazz. Chim. Acta* **1967**, *1*, 172.

(154 000), 447 (112 000), 528 (18 000); FAB$^+$ *m*/*z* (nature of the peak, relative intensity) 2429.2 ([M − PF_6]$^+$, 100), 1142.2 ([M − 2PF_6]$^{2+}$, 20). Anal. Calcd for $C_{104}H_{100}F_{24}N_{12}Os_2P_4S_3$: C, 48.52; H, 3.92; N, 6.53. Found: C, 48.64; H, 3.83; N, 6.25.

RuOs Complex. A Schlenk flask was charged with the **Os** complex (30 mg, 0.02 mmol), [Ru(bpy)$_2$Cl$_2$]·2H$_2$O (13 mg, 0.03 mmol), and finally ethyl alcohol (10 mL). The solution was heated at 90 °C for 3 days, and then the solvent was evaporated under vacuum. The residue was treated with a saturated aqueous solution of KPF_6 (10 mL) and extracted with dichloromethane. The organic extracts were washed with water and dried over absorbent cotton. The solvent was removed by rotary evaporation. The residue was purified by chromatography on alumina, eluting with dichloromethane to dichloromethane−methyl alcohol (97.0/3.0, v/v) to give 33 mg (80%) of **RuOs** as a brown solid: ^{1}H NMR (200 MHz, (CD$_3$)$_2$CO) δ 8.86−8.78 (m, 12H), 8.30−7.95 (m, 24H), 7.65−7.48 (m, 8H), 7.26 (s, 2H), 2.67−2.51 (m, 12H), 1.67−1.21 (m, 24H), 0.95−0.84 (m, 18H); IR (KBr, cm^{-1}) 3113, 3078, 2952, 2930, 2869, 2197, 1594, 1464, 1447, 1374, 1242, 840; UV−vis (CH_3CN) λ nm (ϵ, M^{-1} cm^{-1}) 288 (177 000), 443 (115 000), 530 (11 000); FAB$^+$ *m*/*z* (nature of the peak, relative intensity) 2343.2 ([M − PF_6]$^+$, 90), 1099.2 ([M − 2PF_6]$^{2+}$, 30). Anal. Calcd for $C_{104}H_{100}F_{24}N_{12}OsP_4RuS_3$: C, 50.26; H, 4.06; N, 6.76. Found: C, 50.40; H, 4.03; N, 6.50.

ReOs Complex. A solution of Re(CO)$_5$Cl (9 mg, 0.03 mmol) in toluene (6 mL) was heated at 80 °C for 30 min. This mixture was added to a solution of **Os** (30 mg, 0.02 mmol) in CH_2Cl_2 (6 mL) at 25 °C and heated at 80 °C for 12 h. The solvent was evaporated under vacuum. The residue was treated with a saturated aqueous solution of KPF_6 (10 mL) and extracted with dichloromethane. The organic extracts were washed with water and dried over absorbent cotton. The solvent was removed by rotary evaporation. The residue was purified by chromatography on alumina, eluting with dichloromethane to dichloromethane−methyl alcohol (97.5/2.5, v/v) to give 30 mg (85%) of **ReOs** as a brown solid: ^{1}H NMR (200 MHz, (CD$_3$)$_2$CO) δ 9.13−9.10 (m, 2H), 8.86−8.66 (m, 8H), 8.33−8.24 (m, 2H), 8.12−7.95 (m, 12H), 7.55 (t, ^3J = 7.2 Hz), 7.25 (s, 2H), 2.85−2.78 (m, overlapping with residual water), 2.73−2.51 (m, 12H), 1.70−1.21 (m, 24H), 1.02−0.84 (m, 18H); IR (KBr, cm^{-1}) 3067, 2956, 2928, 2870, 2196, 2021, 1918, 1895, 1592, 1465, 1446, 1377, 1241, 841; UV−vis (CH_3CN) λ nm (ϵ, M^{-1} cm^{-1}) 290 (105 000), 442 (113 000); FAB$^+$ *m*/*z* (nature of the peak, relative intensity) 1943.2 ([M − PF_6]$^+$, 100), 899.1 ([M − 2PF_6]$^{2+}$, 10). Anal. Calcd for $C_{87}H_{84}ClF_{12}N_8O_3OsP_2ReS_3$: C, 50.05; H, 4.06; N, 5.35. Found: C, 49.84; H, 3.76; N, 5.04.

Electrochemical Measurements. Electrochemical studies employed cyclic voltammetry with a conventional three-electrode system using a BAS CV-50W voltammetric analyzer equipped with a Pt microdisk (2 mm^2) working electrode and a silver wire counter electrode. Ferrocene was used as an internal standard and was calibrated against a saturated calomel reference electrode (SCE) separated from the electrolysis cell by a glass frit presoaked with an electrolyte solution. Solutions contained the electroactive substrate in deoxygenated and anhydrous acetonitrile containing tetra-*n*-butylammonium hexafluorophosphate (0.1 M) as the supporting electrolyte. The quoted half-wave potentials were reproducible within ≈20 mV.

Optical Spectroscopy. Absorption spectra of dilute solutions (2×10^{-5} M) of CH_2Cl_2 (for the ligand) and CH_3CN (for the complexes) were obtained with a Perkin-Elmer Lambda 45 UV−vis spectrometer. The luminescence spectra for ca. 2×10^{-5} M air-equilibrated solutions at room temperature and 77 K were measured using an Edinburgh FLS920 spectrometer equipped with a Hamamatsu R5509-72 supercooled photomultiplier tube (193 K), a TM300 emission monochromator with NIR grating blazed at 1000 nm, and an Edinburgh Xe900 450-W xenon arc lamp as the light source. The excitation wavelength was 445 nm; this for the complexes leads to a final population of the lowest-lying emitting levels of Ru- or Os-based metal-to-ligand charge-transfer nature (see the text).[58] Corrected luminescence spectra in the range of 700−1800 nm were obtained by using a correction curve for the phototube response provided by the manufacturer. Luminescence quantum efficiencies (ϕ_{em}) were evaluated by comparing wavelength-integrated intensities (I) with reference to [Ru(bpy)$_3$]Cl$_2$ ($\phi_r = 0.028$ in air-equilibrated water)[59] or [Os(bpy)$_3$](PF$_6$)$_2$ ($\phi_r = 0.005$ in degassed acetonitrile)[60] as standards and by using the following equation:[60,61]

$$\phi_{em} = \frac{A_r \eta^2 I}{\eta_r^2 I_r A} \phi_r \qquad (1)$$

where A and η are absorbance values (<0.15) at the employed excitation wavelength and the refractive index of the solvent, respectively. Band maxima and relative luminescence intensities are obtained with uncertainties of 2 nm and 20%, respectively. The luminescence lifetimes were obtained with the same equipment operated in single-photon mode by using a 407-nm laser diode excitation controlled by a Hamamatsu C4725 stabilized picosecond light pulser. For **ReOs**, an IBH 5000F single-photon equipment was employed, with excitation at 337 nm. Analysis of the luminescence decay profiles against time was accomplished by using software provided by the manufacturers. Estimated errors are 10% on lifetimes and 20% on quantum yields, and the working temperature was either 298 ± 2 K (1-cm^2 optical cells employed) or 77 K (with samples contained in capillary tubes immersed in liquid nitrogen).

The band profiles of the corrected luminescence spectra, $I(E)$, on an energy scale (E, cm^{-1}) were analyzed according to eq 2, describing the relationship between the Franck−Condon envelope and some pertinent parameters.[62−64] with $S = \lambda/\hbar\omega$. In this equation,

$$I(E) = \sum_m \left(\frac{E_0 - m\hbar\omega}{E_0}\right)^3 \frac{S^m}{m!} \exp\left[-4(\ln 2)\left(\frac{E - E_0 + m\hbar\omega}{\Delta\bar{\nu}_{1/2}}\right)^2\right] \qquad (2)$$

E_0 is the energy of the 0−0 transition (the energy gap between the 0−0 vibrational levels in the excited and ground states), m is a vibrational quantum number (in practice, an upper limit $m = 5$ is employed) for a high-frequency mode typical for aromatic rings, $\hbar\omega = 1400$ cm^{-1},[62−64] $\Delta\bar{\nu}_{1/2}$ is the width at half-maximum of the vibronic band, λ and S are the reorganization energy and the displacement parameter, respectively, along those modes, and k_B is the Boltzmann constant. High values for S (typically, >0.7)[65] indicate that the excited state is significantly distorted along the concerned vibrational mode because of electronic *localization*

(58) Yeh, A. T.; Shank, C. V.; McCusker, J. K. *Science* **2000**, *289*, 935.
(59) Nakamaru, K. *Bull. Chem. Soc. Jpn.* **1982**, *55*, 2967.
(60) Kober, E. M.; Caspar, J. V.; Lumpkin, R. S.; Meyer, T. J. *J. Phys. Chem.* **1986**, *90*, 3722.
(61) Demas, J. N.; Crosby, G. A. *J. Phys. Chem.* **1971**, *75*, 991.
(62) Barqawi, K. R.; Murtaza, Z.; Meyer, T. J. *J. Phys. Chem.* **1991**, *95*, 47.
(63) Claude, J. P.; Meyer, T. J. *J. Phys. Chem.* **1995**, *99*, 51.
(64) Murtaza, Z.; Graff, D. K.; Zipp, A. P.; Worl, L. A.; Jones, W. E.; Bates, W. D.; Meyer, T. J. *J. Phys. Chem.* **1994**, *98*, 10504.
(65) Goze, C.; Chambron, J. C.; Heitz, V.; Pomeranc, D.; Salom-Roig, X. J.; Sauvage, J. P.; Morales, A. F.; Barigelletti, F. *Eur. J. Inorg. Chem.* **2003**, 3752.

effects. When the excited state undergoes extended electronic *delocalization*, low *S* values are obtained (typically, in the range of 0.2−0.6),[66] indicating that the electronic curve for the excited level is not much displaced relative to that for the ground state.

Results and Discussion

The schematic structures of the ligand and complexes that are the focus of the present investigation are illustrated in Chart 1. Preparation of the mono- and binuclear complexes was inspired by our previous syntheses of d^6 transition-metal complexes.[53] During these preparations, the ligand was allowed to react with *cis*-Cl[Ru(bipy)$_2$Cl$_2$]·2H$_2$O or *cis*-Cl-[Os(bipy)$_2$Cl$_2$] in refluxing ethanol. Careful separation by chromatography and double recrystallization in adequate solvents allow one to isolate the mono- and binuclear complexes in acceptable yields. The heterobinuclear complexes were best prepared from the mono-osmium complex rather than from the ruthenium complex. The purification of the target complexes is straightforward by column chromatography. In the **ReOs** binuclear complex, the *fac* configuration around the rhenium center was further confirmed by FT-IR exhibiting three intense carbonyl stretching vibrations at 2196, 2021, and 1918 cm^{-1}.[67]

These complexes were unambiguously characterized by ^{1}H NMR, FAB$^+$ MS, and elemental analysis as well as by cyclic voltammetry, UV−vis, and luminescence spectroscopy. The fingerprint of these complexes is shown by the aromatic part of the ^{1}H NMR spectrum; for illustration purposes, Figure 1 compares ^{1}H NMR spectra for **TBTBT**, **Os**, and **OsOs** complexes. For the free ligand, two signals are particularly interesting. One of them relies on the two well-defined doublets found respectively at 8.43 and 8.42 ppm (Figure 1a) and corresponds to the four protons 3 and 3′ on the dissymmetrically substituted bipyridines. The other one is the singlet located at 6.92 ppm, which corresponds to the two terminal thiophene protons. In the case of the **Os** complex, the doublet corresponding to the protons 3 and 3′ on the uncomplexed bipyridine is still present at 8.52 and 8.51 ppm but integrates as expected for two protons compared to one of the thiophene protons (Figure 1b). Furthermore, the presence of two singlets at 7.25 and 7.20 ppm for the thiophene protons confirms the dissymmetrical nature of the molecule and its mononuclear nature.

By saturation of both coordination sites with osmium, the absence of the protons around 8.50 ppm confirms the presence of a symmetric **OsOs** complex (Figure 1c). In addition, only one singlet resonates at 7.25 ppm, and complexation of each metal center imported 16 additional aromatic protons because of the additional unsubstituted bipyridine units. The same features are apparent in the ruthenium or rhenium series. All complexes exhibit intense molecular peaks with the expected isotopic profiles when analyzed by FAB MS.

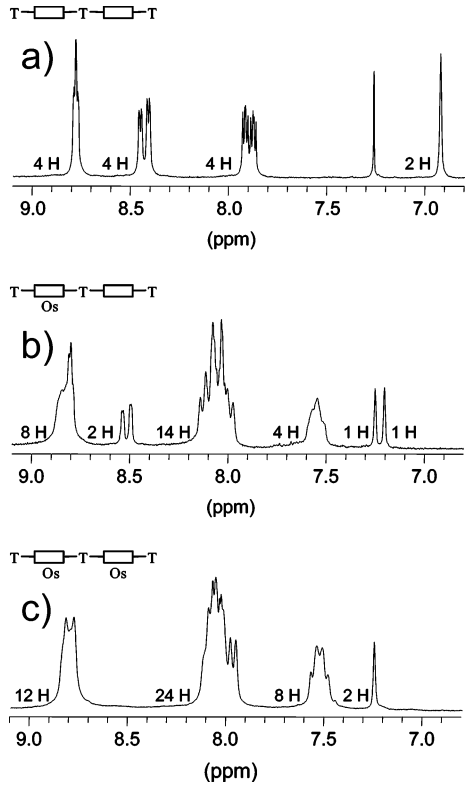

Figure 1. ^{1}H NMR spectra (at 200 MHz) measured at room temperature in $CDCl_3$ for (a) ligand **TBTBT** and in acetone-d_6 for (b) complex **Os** and (c) complex **OsOs**. For the sake of clarity, only the aromatic regions of the spectra are shown. The insets show schematic representations of the molecules.

Electrochemistry. The electrochemical properties of the complexes were characterized by cyclic voltammetry in a CH_3CN solution. Table 1 lists the potentials (relative to the SCE reference electrode) for the waves that were observed in the +1.6 to −2.1 V windows. First, for **Ru** and **RuRu** complexes, a single reversible anodic wave was observed around +1.32 V (+1.34 V for **RuOs**), which is due to the Ru(II/III) couple. Note that, for **RuRu**, the Ru(II/III) wave is found at the same potential versus the mononuclear complex because of the fact that both metal centers are oxidized approximately at the same potential. The observation of a single wave supports the notion that these metal centers are not in strong electronic interaction. The anodic shift in the metal-centered oxidation ($\Delta V = 50$ mV) versus the reference complex likely reflects the σ-withdrawing behavior of the ethynyl junctions. The absence of a more pronounced effect is possibly counterbalanced by the two dibutylthiophene donor groups. There is, however, no indication of dibutylthiophene oxidation within the given electrochemical window.[54] The osmium center is much easier to oxidize versus its ruthenium counterpart, and here also a single oxidation wave is found for the binuclear complex and the anodic shifts ($\Delta V = 60$ mV) are due to similar effects discussed above for the Ru complexes. As would be expected in the absence of a large interaction between metal centers, the heterobinuclear complexes exhibit two oxidation waves because of the presence of two different metal centers (Table 1). For the **ReOs** complex, a reversible oxidation of the Os center is found, whereas a quasi-reversible oxidation is found

(66) Hammarström, L.; Barigelletti, F.; Flamigni, L.; Indelli, M. T.; Armaroli, N.; Calogero, G.; Guardigli, M.; Sour, A.; Collin, J. P.; Sauvage, J. P. *J. Phys. Chem. A* **1997**, *101*, 9061.
(67) Juris, A.; Campagna, S.; Bidd, I.; Lehn, J. M.; Ziessel, R. *Inorg. Chem.* **1988**, *27*, 4007.

Table 1. Electrochemical Properties of Complexes and References in Solution[a]

complex	$E^{0\prime}$(ox, soln) (V), ΔE_p (mV)[b]	$E^{0\prime}$(red, soln) (V), ΔE_p (mV)[c]
Ru	1.32 (60), 1e$^-$	−0.98 (60), 1e$^-$, −1.34 (80), 1e$^-$, −1.69 (irrev)
RuRu	1.32 (60), 2e$^-$	−0.99 (70), 2e$^-$, −1.37 (70), 2e$^-$, −1.73 (irrev)
Os	0.89 (60), 1e$^-$	−0.94 (60), 1e$^-$, −1.26 (80), 2e$^-$, −1.68 (irrev)
OsOs	0.89 (60), 2e$^-$	−0.95 (60), 2e$^-$, −1.29 (70), 2e$^-$, −1.69 (irrev)
RuOs	0.88 (60), 1e$^-$ 1.34 (70), 1e$^-$	−0.95 (60), 2e$^-$, −1.32 (70), 2e$^-$, −1.73 (irrev)
ReOs	0.87 (60), 1e$^-$ 1.36 (90), 1e$^-$	−0.97 (60), 1e$^-$, −1.35 (70), 1e$^-$, −1.70 (irrev.)
$[Ru(bpy)_3]^{2+}$ [d]	1.27 (60)	−1.35 (60), −1.54 (70), −1.79 (70)
$[Os(bpy)_3]^{2+}$ [e]	0.83 (60)	−1.25 (60), −1.54 (70), −1.80 (70)
$[Re(bpy)(CO)_3Cl]$[f]	1.32 (irrev)	−1.35 (60)

[a] The electrolyte was 0.1 M $TBAPF_6$/anhydrous CH_3CN, complex concentration of 1−1.5 mM, at room temperature. All potentials (±10 mV) are reported in volts vs a Pt^0 pseudo reference electrode and using Fc^+/Fc as the internal reference at 0.38 V (ΔE_p = 70 mV). For irreversible processes, the anodic or cathodic peak potentials are provided. The number of involved electrons is estimated from the integration of the reversible processes and is indicated as ne^-. [b] Metal-based oxidation. [c] Successive ligand-localized reduction steps. [d] From ref 69. [e] From ref 100. [f] From ref 68.

for the Re center. The latter oxidation is found to be less anodic (ΔV = 40 mV) and irreversible in *fac*-[Re(bipy)-$(CO)_3Cl$].[68]

Interestingly, all complexes exhibit at least two well-resolved reversible waves in the cathodic branch of the voltammograms, which are due to reductions centered on the substituted and unsubstituted bipyridine ligands. The entries in Table 1 are organized according to the assignment as to which bipyridine ligand is reduced at the listed potential. For each of the complexes, the first reduction is shifted to a more positive potential than the first reduction of $[Ru(bpy)_3]^{2+}$, $[Os(bpy)_3]^{2+}$, and $[Re(bpy)(CO)_3Cl]$ (data shown for comparison). This feature clearly indicates that in all of the new complexes the first reduction is localized on the bridged ligand. Moreover, there are no significant differences in the potentials of the first reduction for the mono- and binuclear complexes. These interesting features indicate similar electronic environments for the two metal centers. Similar behavior is also found for the Os series of complexes when compared to $[Os(bpy)_3]^{2+}$.[69] Likewise, in all complexes of the **TBTBT** ligand, the third reduction likely localized on an unsubstituted bpy is overlapped by a strong adsorption/desorption peak, which hinders the exact potential determination.

Optical Properties. Absorption. Absorption spectra are displayed in Figure 2, and concerned data are collected in Table 2, together with luminescence results to be discussed below. The absorption properties of ligand **TBTBT** have been reported and discussed previously.[54] The band peaking at 278 nm is of $^1\pi\pi^*$ character and is due to transitions centered on the bpy residues. The lowest-energy broad band peaking at 405 nm (extinction coefficient $\epsilon \sim 10^5$ M^{-1} cm^{-1}) is due to an admixture of $^1\pi\pi^*$ transitions for the thiophene backbone[70,71] and of ^{1}CT (charge-transfer) transitions originating from the interaction of alkyl groups with thiophene and acetylenic fragments.[51] In particular, the latter transitions

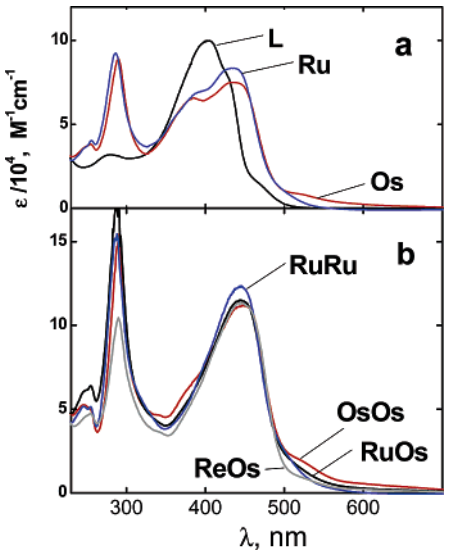

Figure 2. Ground-state absorption spectra. The solvents were CH_2Cl_2 for **TBTBT** and CH_3CN for the complexes. The top panel (a) is for **TBTBT** and the mononuclear species; the bottom panel (b) is for the binuclear species.

are likely associated with the low-energy shoulder at ca. 420 nm.[54]

In Figure 2a are compared the absorption profiles of the ligand **TBTBT** and of the mononuclear Ru- and Os-based species, **Ru** and **Os**. As expected, the intensity of bpy-centered $^1\pi\pi^*$ (^{1}LC) transitions (in the 280−290-nm region) increases upon passing from **TBTBT** to **Ru** and **Os** (ϵ from 32 200 to 92 000 and 88 400 M^{-1} cm^{-1}, respectively) because of the increased number of bpy units. For **Ru** and **Os** and with respect to **TBTBT**, the lowest-energy absorption peak is red-shifted and less intense (434 and 435 nm, with ϵ = 83 500 and 75 200 M^{-1} cm^{-1} for **Ru** and **Os**, respectively); these absorption features are likely ascribable to a mixing of ^{1}MLCT transitions (typically, with $\epsilon \sim$ 10 000−20 000 M^{-1} cm^{-1} [22,72]) and ^{1}CT ligand-centered transitions.[54] For **Os**, an additional absorption tail extending to 650 nm and more (peaking at 530 nm, ϵ = 8000 M^{-1} cm^{-1}) is also registered, owing to formally forbidden ^{3}MLCT absorption transitions.[22,60]

(68) Luong, J. C.; Nadjo, L.; Wrighton, M. S. *J. Am. Chem. Soc.* **1978**, *100*, 5790.
(69) Grosshenny, V.; Harriman, A.; Romero, F. M.; Ziessel, R. *J. Phys. Chem.* **1996**, *100*, 17472.
(70) Becker, R. S.; deMelo, J. S.; Macanita, A. L.; Elisei, F. *J. Phys. Chem.* **1996**, *100*, 18683.
(71) Belletete, M.; Mazerolle, L.; Desrosiers, N.; Leclerc, M.; Durocher, G. *Macromolecules* **1995**, *28*, 8587.
(72) Juris, A.; Balzani, V.; Barigelletti, F.; Campagna, S.; Belser, P.; von Zelewsky, A. *Coord. Chem. Rev.* **1988**, *84*, 85.

Table 2. Absorption and Luminescence Properties of the Ligand and Complexes[a]

	absorption	emission					
		298 K				77 K	
	λ_{max} (nm), ϵ_{max} (M^{-1} cm^{-1})	λ_{em} (nm)	ϕ_{em}	τ (ns)[b]	$10^{-4}k_r$	λ_{em} (nm)	τ (μs)[b]
TBTBT[c]	278 (32 200), 405 (99 900)	560	0.38	<1	>4 × 10^4		<1 × 10^{-3}
Ru	287 (92 000), 434 (83 500)	710	4.2 × 10^{-3}	170	2.5	710	3.8[d]
RuRu	288 (155 000), 444 (123 000)	710	2.9 × 10^{-3}	165	1.8	690	4.2[d]
Os	291 (88 400), 435 (75 200), 530 (8000)	928	8.4 × 10^{-4}	12	7	840	2.0
OsOs	290 (154 000), 447 (112 000), 528 (18000)	928	6.4 × 10^{-4}	12.5	5.1	840	1.8
RuOs	288 (177 000), 443 (115 000), 530 (11000)	928	5.8 × 10^{-4}	11	5.3	840	1.8
ReOs	290 (105 000), 442 (113 000), 530 (10 000)	928	6.0 × 10^{-4}	10	6	840	1.7
$[Ru(bpy)_3]^{2+}$ [e]	288 (76 600), 452 (14 600)	615	1.5 × 10^{-2}	170	8.8	582	5.0
$[Os(bpy)_3]^{2+}$ [f]	290 (78 000), 478 (11 100), 579 (3300)	743	3.2 × 10^{-3}	49	6.5	710	0.8
$[Re(bpy)(CO)_3(H_2O)]^{+}$ [g]	288 (~23 000), ~320 (~13 000)	530	1.2 × 10^{-2}	62	19.4	500	0.14

[a] In air-equilibrated solvents, CH_2Cl_2 for the **TBTBT** ligand and CH_3CN for the complexes, at the indicated temperature; λ_{exc} = 445 nm for the luminescence spectra and 407 nm for the lifetimes; for emission measurements of **ReOs**, λ_{exc} was 337 nm. [b] Values obtained by monitoring the luminescence peak; single-exponential decays were observed in each case. [c] Some values are different from those reported in ref 54. [d] A minor, long-lived (30−50-μs) contribution is also present. [e] From refs 72 and 101. [f] From refs 60 and 102. [g] From ref 103; it may be noticed that replacement of Cl^- for H_2O is expected to cause red-shifting of the Re-to-L CT bands, both for absorption and emission; see, for instance, ref 104.

The absorption spectra (Figure 2b) for the homometallic binuclear species, **RuRu** and **OsOs**, and for the heterometallic species, **ReOs** and **RuOs**, feature intense bands due to both (i) transitions centered at the bpy units (in the region 288−290 nm, with $\epsilon \sim$ 154 000−177 000 M^{-1} cm^{-1} for **RuRu**, **OsOs**, and **RuOs** and ϵ = 105 000 M^{-1} cm^{-1} for **ReOs**, whose absorption intensity is lower with respect to the other binuclear complexes because of a reduced number of bpy units) and (ii) the likely overlap of ^{1}LC and ^{1}MLCT transitions (in the region 443−447 nm, with $\epsilon \sim$ 112 000−123 000 M^{-1} cm^{-1}). Clearly, with respect to the mononuclear cases **Ru** and **Os**, the more intense transitions in **RuRu**, **OsOs**, **RuOs**, and (partly) **ReOs** are due to the increased number of bpy units because of the higher nuclearity. For all of the complexes examined, it may be noticed that the peak maximum encompassing ^{1}MLCT contributions is always in a narrow range, 434−447 nm (see Figure 2 and Table 2). In a broad sense, this could indicate that the metal-based component units in the binuclear species are not strongly interacting, as is also suggested by the electrochemical results (see above). On the other hand, the fact that ligand-based transitions are also present in this spectral region may lead to masking effects, and the available optical absorption data do not help to reach a firm conclusion about the intermetal interaction. For the Os-containing binuclear complexes **OsOs**, **RuOs**, and **ReOs**, an absorption tail, of ^{3}MLCT nature and extending to ca. 670 nm, is also present, as is observed for the mononuclear complex **Os** (see Figure 2 and Table 2).

Luminescence. Luminescence results are gathered in Table 2, and luminescence spectra are illustrated in Figure 3, with panel a for room temperature and panel b for 77 K cases; excitation was performed at 445 nm (for **ReOs**, excitation was at 337 nm). Ligand **TBTBT** exhibits room-temperature luminescence features (λ_{em} = 560 nm, ϕ_{em} = 0.38, and τ < 1 ns, with CH_2Cl_2 solvent) that are typical for the fluorescence of thiophene-based oligomers.[40,50,70,71,73] For all of the complexes investigated, the intense oligothiophene-based fluorescence disappears and is replaced by a weaker luminescence (Table 2).

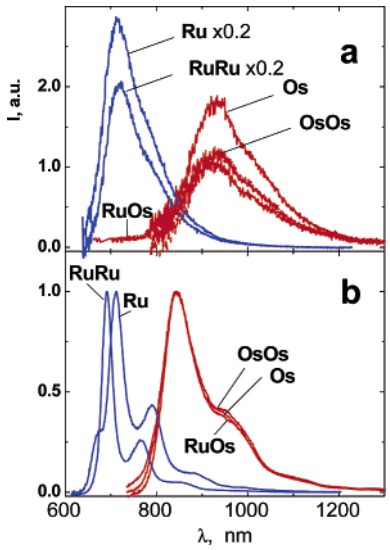

Figure 3. Luminescence spectra of the indicated complexes, solvent CH_3CN, λ_{exc} = 445 nm in all cases. The spectral profiles are corrected for the phototube response; see the Experimental Section. The top panel (a) is for isoabsorbing samples at room temperature; the bottom panel (b) shows normalized samples.

For **Ru** and **RuRu** at room temperature, the luminescence profiles (Figure 3), the energy position of the luminescence bands (peaking at much lower energy than for $[Ru(bpy)_3]^{2+}$; Table 2), and the luminescence efficiencies and lifetimes are consistent with a ^{3}(Ru → **TBTBT**) CT nature for the emission. This implies that the CT emission level is not spatially confined to the bpy residue (of **TBTBT**) directly coordinated at the metal center but spreads over the various fragments of **TBTBT**. This is also in accord with the electrochemical results, indicating that a much easier reduction (by ~0.35 V) is centered at the **TBTBT** ligand with respect to bpy, which is, of course, ascribable to the different extent of delocalization of the concerned lowest unoccupied molecular orbitals (LUMOs). Interestingly, the mononuclear complex **Ru** exhibits a stronger luminescence intensity than its binuclear homometallic counterpart **RuRu**, ϕ_{em} = 4.2 × 10^{-3} and 2.9 × 10^{-3}, respectively, at room temperature;

(73) van Hal, P. A.; Knol, J.; Langeveld-Voss, B. M. W.; Meskers, S. C. J.; Hummelen, J. C.; Janssen, R. A. J. *J. Phys. Chem. A* **2000**, *104*, 5974.

notice, however, that the peak positions and lifetimes are quite similar (Table 2). Thus, even if the intermetal interaction seems not strong (which would also affect the energy position of the emission band), this clearly reflects some electronic change consequent to the addition of the second metal center. Results for the luminescence of **Ru** and **RuRu** at 77 K indicate predominant contributions from ^{3}MLCT levels but also contributions from ^{3}LC levels. This is suggested by both observation of structured luminescence profiles (Figure 3b) and dual exponential decays for the emission, with shorter-lived contributions of $\sim$4 μs and longer-lived ones, on the scale of several tens of microseconds (see Table 2). It may be noticed that, upon passing from room temperature to 77 K, while the mononuclear **Ru** complex exhibits no change in the emission maximum (710 nm), for **RuRu** a small blue shift occurs (from 710 to 690 nm; Table 2). This behavior seems to indicate that the MLCT emission includes larger LC contributions for **Ru** than for **RuRu**.

For the Os-containing complexes **Os** and **OsOs**, a comparison with the literature results for $[Os(bpy)_3]^{2+}$ and other Os(II)-containing complexes[60] allows the assignment of the luminescence properties to ^{3}(Os $\rightarrow$ **TBTBT**) CT excited states. Again, the mononuclear complex **Os** exhibits a stronger luminescence intensity than its binuclear homometallic counterpart **OsOs**, $\phi_{em} = 8.4 \times 10^{-4}$ and 6.4×10^{-4}, respectively, at room temperature (however, the peak positions and lifetimes are quite similar; Table 2). At 77 K, the luminescence spectra of **Os** and **OsOs** exhibit overlapping profiles (Figure 3b) and quite similar lifetimes, $\tau = 2.0$ and 1.8 μs, respectively (Table 2). Upon passing from room temperature to 77 K, both complexes exhibit a blue shift of the emission maximum (from 928 to 840 nm; Table 2), as is expected on the basis of the MLCT character of the emission.[60]

For the heterometallic binuclear complex **RuOs**, use of light at 445 nm is expected to result in the population of ligand centered (^{1}LC), Ru-centered (^{1}RuLCT), and Os-centered (^{1}OsLCT) levels (see Figure 2). Judging from the absorption profiles displayed in this figure, it seems reasonable to assume that (i) only a small fraction of light (<25%) is directly absorbed by **TBTBT** at 445 nm (with the formation of ^{1}LC states) and that (ii) the larger fraction of light (>75%) is further subdiveded between the metal-containing chromophores with the formation of ^{1}MLCT states, i.e., for **RuOs**, between Ru and Os centers in an approximate 1:1 ratio. For **RuOs**, the registered room-temperature luminescence band peak, intensity, and lifetime ($\lambda_{em} = 928$ nm, $\phi_{em} = 5.8 \times 10^{-4}$, and $\tau = 11$ ns, respectively) are ascribable of ^{3}(Os $\rightarrow$ **TBTBT**) CT nature and no Ru-based luminescence is detected (see Figure 3). The same is true for the 77 K results. This, together with the fact that the Os-based luminescence intensity of **RuOs** is practically the same as that exhibited by the homometallic binuclear complex **OsOs** ($\phi_{em} = 6.4 \times 10^{-4}$), indicates that full Ru $\rightarrow$ Os energy transfer takes place (see the discussion below). A similar line of reasoning applies for the case of **ReOs**. For this complex, excitation at 337 nm is expected to result in population of ^{1}ReLCT, ^{1}OsLCT, and ^{1}LC levels. However, because of the lack of a useful mononuclear Re-based reference complex, we could not obtain a safe estimate of the concerned absorption ratios. In this case, the only useful observation is that only an Os-based emission is detected (suggesting a complete Re $\rightarrow$ Os energy transfer) at both room temperature and 77 K; see the results in Table 2.

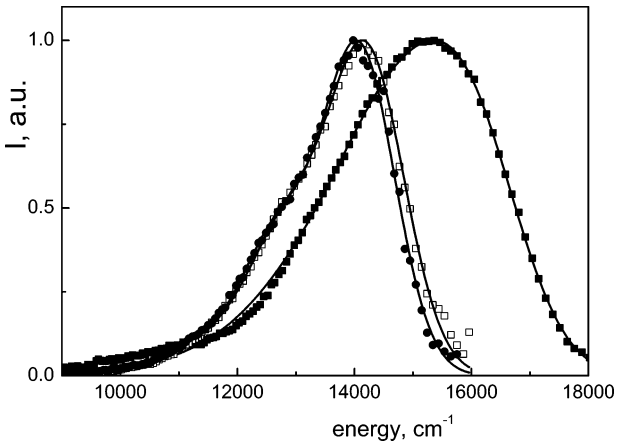

Figure 4. Vibronic analysis of the room-temperature normalized luminescence profiles for $[Ru(bpy)_3]^{2+}$ (■), **Ru** (□), and **RuRu** (●). The results from fits according to eq 2 of the text are drawn as full lines.

Table 3. Data from Vibronic Analysis of the Luminescence Spectra of the Complexes[a]

	E^0 (cm^{-1})	S[b]	$\hbar\omega$ (cm^{-1})	$\Delta\bar{\nu}_{1/2}$[c] (cm^{-1})
Ru	14 200	0.59	1400	1530
RuRu	14 080	0.57	1400	1450
Os	11 100	0.46	1400	1700
OsOs	11 300	0.50	1400	1900
RuOs	11 300	0.50	1400	1900
$[Ru(bpy)_3]^{2+}$	15 920	1.07	1400	2080
$[Os(bpy)_3]^{2+}$	13 600,[d] 13 510[e]	0.68,[d]0.75[e]	1350,[d] 1300[e]	1550

[a] According to eq 2 of the text; at room temperature, in CH_3CN, excitation was performed at 445 nm. [b] Displacement parameter $S = \lambda/\hbar\omega$. [c] Full width at half-maximum. [d] From ref 64. [e] From ref 60.

Vibronic analysis of the luminescence profiles for the complexes provides interesting hints about the extent of electronic delocalization of the emitting ^{3}MLCT level.[3,62−66] Figure 4 shows the results for the room-temperature cases of **Ru**, **RuRu**, and $[Ru(bpy)_3]^{2+}$, as are obtained by fitting eq 2 of the Experimental Section to their luminescence spectra. Table 3 collects values for the E_0, λ, and S parameters along the CC and CN vibrational modes $\hbar\omega$ that contribute to deactivation of the CT emissive level ($\hbar\omega$ is taken 1400 cm^{-1} as an average[3,62−66]). Here, E_0 is the energy of the 0−0 transition, and λ and S are the reorganization energy and the displacement parameter, respectively, along the concerned vibrational modes; see the Experimental Section. In particular, the low S value for complexes **Ru** and **RuRu** ($S \sim 0.6$; see Table 3), as compared to that for $[Ru(bpy)_3]^{2+}$ ($S = 1.07$), suggests that the electronic curve for the emissive level of the former complexes is not much displaced relative to that for the ground state. This effect is due to the effective electronic delocalization of the emissive MLCT state because of the large size of the ligand,[66,74] as is the case here for **TBTBT**.[54] When the emission is Os-based, such an effect

is still present with $S \sim 0.7$ for $[Os(bpy)_3]^{2+}$ and $S \sim 0.5$ for the Os-based emitters investigated here; see Table 3. In this case, however, delocalization effects at the ligand are expected to be somewhat masked by the pronounced π-back-bonding interaction between the highest occupied molecular orbital (HOMO; metal-centered) and LUMO (ligand-centered), typical for osmium(II) polypyridine complexes.[60,64]

Energy Transfer. From the E_0 values collected in Table 3, one sees that the energy gap between the Ru- and Os-based luminescent levels is $\Delta E_0 \sim 0.36$ eV; the energy gap between Re- and Os-based emissive levels, as estimated from the emission maxima listed in Table 2, is even larger. On these bases, for the heterometallic cases **ReOs** and **RuOs**, photoexcitation with $\lambda = 337$ and 445 nm, respectively, offers the possibility of investigating the nature of the Re $\rightarrow$ Os and Ru $\rightarrow$ Os energy-transfer processes. In the former case, however, as mentioned above, a useful mononuclear Re-based complex was not available; thus, we restrict ourselves to a discussion of the results for **RuOs**. For this complex, after excitation at 445 nm, where both the Ru- and Os-based components are excited (see Figure 2), no residual Ru-based luminescence is detected and the emission is solely of Os-based nature (see Table 2 and Figure 3). In addition, the fact that the emission efficiency for **RuOs** is practically the same as that for **OsOs**, $\phi_{em} = 5.8 \times 10^{-4}$ and 6.4×10^{-4}, respectively, is consistent with complete Ru $\rightarrow$ Os energy transfer for the portion of light absorbed at the Ru(II) unit of **RuOs**. An estimate of the Ru $\rightarrow$ Os intramolecular energy-transfer rate constant can usually be obtained from[22,23,75−82]

$$k_{en} = \frac{1}{\tau} - \frac{1}{\tau_0} \tag{3}$$

where τ is the lifetime of the quenched Ru-based emission due to the occurrence of Ru $\rightarrow$ Os energy transfer and τ_0 is the Ru-based unquenched lifetime of a suitable reference donor by taking **RuRu** as such a model, $\tau_0 = 165$ ns (see Table 2). Given that we could not detect any Ru-based emission for **RuOs**, an equivalent expression in terms of emission intensities can be used (eq 4).

$$k_{en} = \frac{1}{\tau_0}\left(\frac{I_0}{I} - 1\right) \tag{4}$$

Here, the ratio of the Ru-based intensities for **RuRu** (I_0) and **RuOs** (I) is taken prudentially as $I_0/I = 10$, in view of an experimental uncertainty of 10% for emission intensity measurements (see the Experimental Section). This yields an experimental rate constant $k_{en} \geq 5.5 \times 10^7$ s^{-1} for the intramolecular Ru $\rightarrow$ Os energy transfer, and below we address the nature of such a process.

Approaches are available to determine the type of energy transfer, which are based on calculations for cases of weakly interacting partners;[83−87]— thus, concerned expressions for rate constants are derived from application of the Golden Rule (eq 5).[84]

$$k = \frac{4\pi^2}{h} H^2 \mathrm{FC} \tag{5}$$

Here, H^2 is the electronic interaction term between the initial and final states and FC is the Franck−Condon factor describing the overlap between the donor and acceptor vibrational modes that are coupled to energy transfer. Even if quantum-mechanical approaches may afford the FC factor for cases of double electron transfer,[64,88−90] rate expressions can be conveniently cast in terms of thermodynamic and spectroscopic quantities[91] (however, the electronic interaction term H cannot be easily calculated[92,93]). According to this classical approach, expressions for double electron transfer (through-bond, Dexter), k_{en}^D, or dipole−dipole (through-space, Förster), k_{en}^F, make use of overlap integrals, J_D and J_F, respectively, that are calculated from emission $F(\bar{\nu})$ and absorption $\epsilon(\bar{\nu})$ spectra, as taken on an energy scale, i.e., wavenumbers, $\bar{\nu}$.

$$k_{en}^D = \frac{4\pi^2 H^2}{h} J_D \tag{6}$$

and

$$k_{en}^F = \frac{8.8 \times 10^{-25} K^2 \phi}{\eta^4 \tau d^6} J_F \tag{7}$$

with

$$J_D = \frac{\int F(\bar{\nu})\, \epsilon(\bar{\nu})\, \mathrm{d}\bar{\nu}}{\int F(\bar{\nu})\, \mathrm{d}\bar{\nu} \int \epsilon(\bar{\nu})\, \mathrm{d}\bar{\nu}}$$

and

$$J_F = \frac{\int F(\bar{\nu})\, \epsilon(\bar{\nu})/\bar{\nu}^4\, \mathrm{d}\bar{\nu}}{\int F(\upsilon)\, \mathrm{d}\bar{\nu}}$$

In eq 7, K^2 is an orientation factor[94] (taken as $^2/_3$ for statistical reasons[87]), ϕ and τ (in nanoseconds) are the

(74) Treadway, J. A.; Loeb, B.; Lopez, R.; Anderson, P. A.; Keene, F. R.; Meyer, T. J. *Inorg. Chem.* **1996**, *35*, 2242.
(75) Barigelletti, F.; Flamigni, L.; Collin, J. P.; Sauvage, J. P. *Chem. Commun.* **1997**, 333.
(76) Keene, F. R. *Coord. Chem. Rev.* **1997**, *166*, 121.
(77) De Cola, L.; Belser, P. *Coord. Chem. Rev.* **1998**, *177*, 301.
(78) Barigelletti, F.; Flamigni, L. *Chem. Soc. Rev.* **2000**, *29*, 1.
(79) Harriman, A.; Ziessel, R. *Chem. Commun.* **1996**, 1707.
(80) Chiorboli, C.; Bignozzi, C. A.; Scandola, F.; Ishow, E.; Gourdon, A.; Launay, J. P. *Inorg. Chem.* **1999**, *38*, 2402.
(81) Weldon, F.; Hammarstrom, L.; Mukhtar, E.; Hage, R.; Gunneweg, E.; Haasnoot, J. G.; Reedijk, J.; Browne, W. R.; Guckian, A. L.; Vos, J. G. *Inorg. Chem.* **2004**, *43*, 4471.
(82) Scandola, F. In *Encyclopedia of Supramolecular Chemistry*; Atwood, J. L., Steed, J. W., Eds.; Marcel Dekker: New York, 2004; p 535.
(83) Van Der Meer, B. W.; Coker, G., III; Chen, S.-Y. S. *Resonance Energy Transfer. Theory and Data*; VCH Publishers: New York, 1994.
(84) Orlandi, G.; Monti, S.; Barigelletti, F.; Balzani, V. *Chem. Phys.* **1980**, *52*, 313.
(85) Sigman, M. E.; Closs, G. L. *J. Phys. Chem.* **1991**, *95*, 5012.
(86) Closs, G. H.; Johnson, M. D.; Miller, J. R.; Piotrowiak, P. *J. Am. Chem. Soc.* **1989**, *111*, 3751.
(87) Serpa, C.; Arnaut, L. G.; Formosinho, S. J.; Naqvi, K. R. *Photochem. Photobiol. Sci.* **2003**, *2*, 616.
(88) Harcourt, R. D.; Scholes, G. D.; Ghiggino, K. P. *J. Chem. Phys.* **1994**, *101*, 10521.
(89) Yeow, E. K. L.; Ghiggino, K. P. *J. Phys. Chem. A* **2000**, *104*, 5825.
(90) Jenkins, R. D.; Andrews, D. L. *Photochem. Photobiol. Sci.* **2003**, *2*, 130.

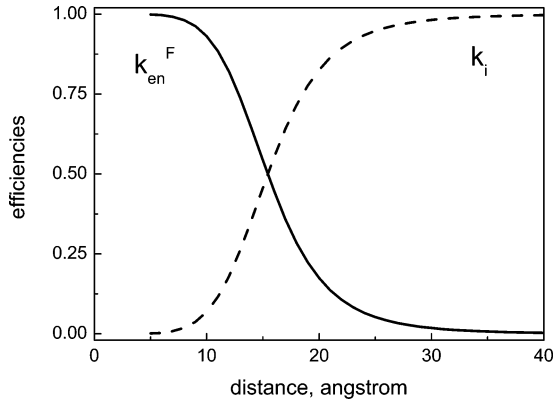

Figure 5. Efficiency of the energy transfer vs intermetal separation in **RuOs** as estimated according to the Förster mechanism and the available spectroscopic results (see the text). The evaluated critical transfer radius is $R_C = 15.4$ Å.

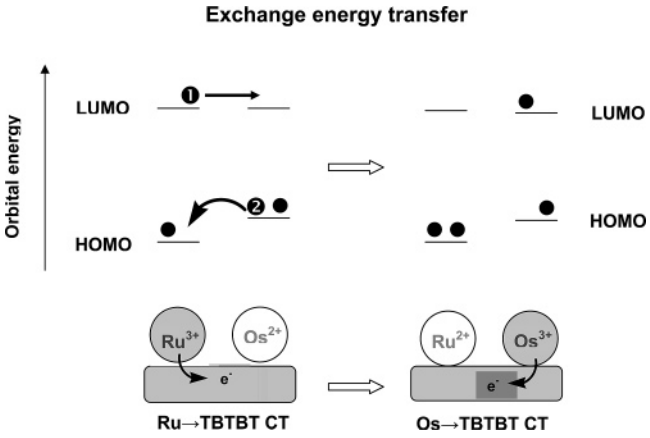

Figure 6. Pictorial description of the double electron energy transfer (Dexter) with the Ru → **TBTBT** CT state (left, shadowed in gray) and the Os → **TBTBT** CT state (right, shadowed in gray) having the promoted electron spread over the shared ligand. According to a schematic view, the energy-transfer step reduces to an exothermic Ru → Os hole transfer (or, equivalently, to an Os → Ru electron transfer; see the text).

emission efficiency and lifetime, respectively, of the excitation donor, η is the refractive index of the solvent, and d (in centimeters) is the distance separation of the interacting donor and acceptor partners. These equations provide useful hints about the nature of the energy transfer, even if some caution is usually taken for processes occurring at short distances, <10 Å. For multicomponent systems incorporating ruthenium(II) and osmium(II) polypyridine centers, the Ru → Os energy transfer is exothermic by 0.2−0.4 eV, and both Dexter- and Förster-type mechanisms have been found to occur.[21,22,29,76−79,95,96] When the bridging ligand is involved (Dexter), superexchange[22,82] or direct-injection mechanisms[53,95] are conceivable. On the basis of consideration of energetic factors,[53] the latter case is not taken into account here.

For the case of **RuOs**, use of the available spectroscopic quantities (see Table 2) allows one to obtain estimates for the overlap integrals, $J_D = 2.7 \times 10^{-4}$ cm and $J_F = 2.5 \times 10^{-14}$ cm^3 M^{-1}. Regarding the Förster mechanism (eq 7), this results in a distance dependence of the energy-transfer efficiency, η_{en}^F (eq 8), which is illustrated in Figure 5.

$$\eta_{en}^F = \frac{k_{en}^F}{k_{en}^F + k_i} \tag{8}$$

In the above equation, k_i is the intrinsic deactivation rate constant of the Ru(II)-based luminophore, i.e., $k_i = 1/\tau$, with $\tau = 165$ ns (Table 2). Notice that, according to the Förster approach, the critical transfer radius is evaluated as $R_C = 15.4$ Å (see Figure 5; this is the interchromophoric distance at which k_{en}^F is equal to the intrinsic deactivation at the donor, k_i).

Molecular modeling results for **RuOs** suggest an intermetal distance of ∼17 Å, and inspection of Figure 5 reveals that at this distance separation of the Ru-based luminescence intensity in **RuOs** is expected to decrease to ca. 40% of that of a suitable Ru-based complex (**Ru** or **RuRu**), with an estimated $k_{en}^F \sim 3 \times 10^6$ s^{-1}. By contrast, for **RuOs** complete disappearance of the Ru(II)-based luminescence is experimentally registered (with $k_{en} \geq 5.5 \times 10^7$ s^{-1}; see above), which rules out the Förster mechanism as being responsible for energy transfer in this binuclear species.[97]

The alternative mechanism for energy transfer to be considered here is the double electron transfer (Dexter), which occurs via through-bond mediation.[22,49,53,82,95,98] From previously obtained optical results for a series of dimeric, trimeric, pentameric, and decameric ligands containing the bpy−ethynylene−thiophene repeat units, we have already seen that the π-electron conjugation increases with the size of the ligand.[54] On the other hand, the vibronic analysis of the luminescence profiles discussed above indicates that, for the luminescent MLCT excited levels of both the mono- and binuclear species investigated, there is a large and similar extent of electronic delocalization at the **TBTBT** ligand. Taken together, these observations suggest that, for the case of excited **RuOs**, the double electron energy transfer, (Ru^{3+}/$^-$**TBTBT**/Os^{2+}) → (Ru^{2+}/**TBTBT**$^-$/Os^{3+}), might be described by the schematic drawing depicted in Figure 6. Given that the promoted electron after the MLCT event is largely delocalized over the **TBTBT** frame, the Ru → Os energy-transfer step could be viewed as actually driven by the intermetal hole-transfer step.[90,99] On the basis of the Ru-

(91) Dexter, D. L. *J. Chem. Phys.* **1953**, *21*, 836.
(92) Förster, T. In *Modern Quantum Chemistry*; Sinanonoglou, O., Ed.; Academic Press: New York, 1965; Vol. III.
(93) Lakowicz, J. R. *Principles of Fluorescence Spectroscopy*; Kluwer Academic/Plenum Publishers: New York, 1999; Chapter 15.
(94) Scholes, G. D. *Annu. Rev. Phys. Chem.* **2003**, *54*, 57.
(95) Benniston, A. C.; Harriman, A.; Li, P. Y.; Sams, C. A. *J. Am. Chem. Soc.* **2005**, *127*, 2553.
(96) Browne, W. R.; O'Boyle, N. M.; McGarvey, J. J.; Vos, J. G. *Chem. Soc. Rev.* **2005**, *34*, 641.
(97) Actually, the geometric factor of eq 7, K^2, can vary between 0 and 4, depending on the spatial alignment (not known to us) of the transition dipoles of the donating and accepting partners; however, even for $K^2 = 4$, $k_{en}^F < k_{en}^D$, vide infra.
(98) Weiss, E. A.; Tauber, M. J.; Kelley, R. F.; Ahrens, M. J.; Ratner, M. A.; Wasielewski, M. R. *J. Am. Chem. Soc.* **2005**, *127*, 11842.
(99) Barigelletti, F.; Flamigni, L.; Guardigli, M.; Juris, A.; Beley, M.; Chodorowski-Kimmes, S.; Collin, J. P.; Sauvage, J. P. *Inorg. Chem.* **1996**, *35*, 136.
(100) Grosshenny, V.; Harriman, A.; Hissler, M.; Ziessel, R. *J. Chem. Soc., Faraday Trans.* **1996**, *92*, 2223.

(III/II) and Os(III/II) reduction potentials (Table 1), this step is formally exothermic by more than 0.4 eV, which compares well with the energy gap between the Ru- and Os-based emission levels, $\Delta E_0 \sim 0.36$ eV (Table 3).

Conclusions

The hybrid systems studied here integrate **TBTBT**, a rigid, conjugated thiophene−ethynylbipyridine backbone and electroactive and photoactive metal−polypyridine centers based on Re(I), Ru(II), and Os(II). At odds with previously investigated cases where the metal-based units appear as terminals of the thiophene-containing wire,[10,38−48] here these units are side-coupled to the **TBTBT** backbone. The electrochemical and spectroscopic results obtained for the investigated series of mono- and binuclear complexes are consistent with weak electronic interactions between the metal centers for the binuclear cases. Nevertheless, because of the extended conjugation at the connecting thiophene−ethynylbipyridine backbone, facile Ru → Os (and, likely, Re → Os) energy transfer takes place between the metal centers of **RuOs** (and, likewise, **ReOs**), which are separated by ∼17 Å. The nature of the energy-transfer process in **RuOs** has been discussed in terms of a double electron exchange mechanism (whereby the constituent electron and hole transfers appear to exhibit some peculiar aspects), as mediated by the **TBTBT** backbone. Thus, the study of this new type of compound provides useful grounds in view of the exploitation of hybrid materials integrating metal units and oligothiophene backbones.

Acknowledgment. This research was supported by the CNRS, le Ministère de la Recherche et des Nouvelles Technologies, by the CNR project PM-P03-ISTM-C4/PM-P03-ISOF-M5 (Componenti molecolari e supramolecolari o macromolecolari con proprietà fotoniche ed optoelettroniche), and by the FIRB project RBNE019H9K "Molecular Manipulation for Nanometric Devices" of MIUR.

IC051717W

(101) Balzani, V.; Bardwell, D. A.; Barigelletti, F.; Cleary, F. L.; Guardigli, M.; Jeffery, J. C.; Sovrani, T.; Ward, M. D. *J. Chem. Soc., Dalton Trans.* **1995**, 3601.

(102) De Cola, L.; Balzani, V.; Barigelletti, F.; Flamigni, L.; Belser, P.; Von Zelewsky, A.; Frank, M.; Vögtle, F. *Inorg. Chem.* **1993**, *32*, 5228.

(103) Encinas, S.; Bushell, K. L.; Couchman, S. M.; Jeffrey, J. C.; Ward, M. D.; Flamigni, L.; Barigelletti, F. *J. Chem. Soc., Dalton Trans.* **2000**, *11*, 1783.

(104) Bardwell, D. A.; Barigelletti, F.; Cleary, R. L.; Flamigni, L.; Guardigli, M.; Jeffery, J. C.; Ward, M. D. *Inorg. Chem.* **1995**, *34*, 2438.